Long-Term Trends in Significant Wave Heights in The Mediterranean as an Indicator of Climate Change

Ahmed S.A. Ibrahim[1], Anas M. El-Molla[1,2], Hany G.I. Ahmed[1]

The Mediterranean coastal zones, particularly along the Nile Delta, are increasingly vulnerable to the impacts of climate change. This study examines the historical changes in the significant wave height along the Nile Delta coast over the past 84 years (1940-2023) at a depth of 20 meters. By synthesizing a comprehensive long-term wave data series using ERA5 reanalysis data and the MIKE21-SW model, the study establishes a robust foundation for analysis. To ensure accuracy, the observed wind data were contrasted against ERA5 data, and they were found to be similar to a great extent. Furthermore, the model's accuracy was rigorously validated against the observational data, ensuring the reliability of the results. Three methods were used to obtain the trends for the maximum wave height to ensure robust and reliable trend assessments (i.e., linear regression, Theil-Sen, and ElasticNet). The results were obtained and analyzed, revealing a statistically significant increase in the maximum wave heights during the study period. Particularly, seasonal analysis revealed a positive trend in maximum wave heights during winter and spring (0.15 to 0.67 cm/year respectively). Furthermore, the monthly analysis showed a positive trend in the wave heights for all months except July, August, and September. Specifically, there were notable increases from September to December, ranging from 0.24 to 0.92 cm/year. These findings are consistent with the global trends of increasing wave heights due to climate change. It is essential for developing adaptive coastal management strategies and designing resilient structures. Consequently, the results will assist coastal authorities in mitigating the impacts of climate change on coastal zones.

KEY WORDS

~ Climate change
~ Wave height
~ Mediterranean
~ Nile delta
~ Long-term trend
~ Numerical Simulation

[1] Al-Azhar University, Faculty of Engineering, Civil Engineering Department, Cairo, Egypt
[2] Galala University, Faculty of Engineering, Civil Engineering Department, Suez, Egypt
e-mail: ahmedsayed.90@azhar.edu.eg
doi: 10.7225/toms.v13.n02.015

Received: 11 Mar 2024 / Revised: 12 Aug 2024 / Accepted: 28 Aug 2024 / Published: 21 Oct 2024

1. INTRODUCTION

Coastal zones, often attracting significant public interest due to their development and urbanization potential, typically result in high population densities (Kovačić and Favro, 2024; Satterthwaite, 2007). However, these areas are particularly vulnerable by the adverse effects of climate change (Albanai, 2020). For instance, Aucan (2018) emphasizes the necessity of regional research to understand how local changes impact hydrodynamics. In this context, understanding wave climate is crucial for assessing the implications of climate change on coastal ecosystems, communities, and infrastructure. Waves play a pivotal role in shaping coastal morphology and influencing near-shore processes, as highlighted by the IPCC (2013). Significant wave height "H_s" is especially important for coastal engineering projects, offshore structures, and various maritime activities (Aydoğan and Ayat, 2018).

Numerous studies have analyzed H_s trends using ERA5 reanalysis data, including the work by Caloiero, Aristodemo, and Ferraro (2022). Additionally, researchers such as Hemer *et al*. (2013), Mentaschi *et al*. (2017), and Soukissian *et al*. (2018) have investigated global changes in wave energy and height. In the Mediterranean region, studies by Lionello *et al*. (2006) and Cannaby and Hüsrevolu (2009), among others, have explored the impact of cyclones and the long-term variability of waves. Recent research has also employed numerical models to predict extreme wave occurrences and assess coastal hazards (Ibrahim *et al*., 2024; Pang *et al*., 2023; Saraçoğlu *et al*., 2016).

Despite these advances, there is a notable lack of data on wave climate along Egypt's coast. Amarouche *et al*. (2019) highlighted the limited and often inaccurate data available for the Egyptian coastline. Similarly, Elkut *et al*. (2021) emphasized the urgent need for developing wave forecasting models to mitigate potential hazards. Understanding long-term changes in ocean waves is essential for analyzing climate dynamics and their societal and economic impacts. Researchers have focused on historical data analysis and future scenario projections using climate models (Chowdhury *et al*., 2019; Grabemann and Weisse, 2008; Wang and Swail, 2002). For example, Ian R. Young and Ribal (2019) identified a global increase in mean H_s from 1985 to 2018, noting an annual rise in mean H_s by 0.3-1 cm/year. Similarly, Shi *et al.* (2024) observed a global increase in H_s associated with the tropical cyclones by approximately 3% per decade. Specifically, in the Mediterranean Sea, studies have reported an overall increase in mean wave energy over the past 40 years, with distinct trends in certain areas (Caloiero *et al*., 2022).

Recent research has further highlighted seasonal and spatial variations in the wave trends across the Mediterranean Sea. For example, Elshinnawy and Antolínez (2023) conducted an analysis covering 58 years from 1961 to 2018, examining both mean and extreme waves in the region. They observed relatively mild long-term trends in Hs, with increases of up to 6 cm per decade. Similarly, Aristodemo *et al.* (2024) reported increasing trends in both the mean and maximum H_s, as well as in Peak Wave Period "T_p". Although there is some debate regarding the trends in the mean H_s, as noted by Amarouche *et al*. (2022), other studies, such as De Leo *et al.* (2024), have identified significant trends in the extreme wave values in specific regions. This body of work underscores the critical importance of understanding wave behavior and trends, particularly in the context of a changing climate.

Based on this framework, the current study investigates the impact of climate change on Hs in the Mediterranean, focusing specifically on the Nile Delta region. By leveraging high-resolution ERA5 reanalysis data and employing the MIKE 21-SW model, the study constructs an extensive 84-year dataset, providing a robust foundation for analyzing long-term wave height trends. Understanding these variations is crucial for developing adaptive coastal management strategies and designing structures that can withstand evolving wave conditions. Furthermore, to ensure a thorough and unbiased trend analysis, three trend estimation methods are used (i.e., linear regression, Theil-Sen, and ElasticNet). This multi-method approach enhances the robustness

of trend detection by addressing the limitations inherent in each technique and ensuring a comprehensive assessment of the wave height trends.

2. MATERIAL AND METHODS

2.1. Study Area

Among the notable works on the Mediterranean, Amarouche *et al.* (2019) documented that it is a semi-enclosed basin connected to the Atlantic via the Strait of Gibraltar. This geographic feature, combined with human activities and the impacts of climate change, has heightened the susceptibility of the Mediterranean coastal regions to various hazards, as noted by Simav *et al.* (2013). Furthermore, Knobler *et al.* (2022) highlighted that the Eastern Mediterranean, including the Nile Delta region, is a significant climate hotspot necessitating focused investigation.

The study area, specifically the Nile Delta, spans a coastal length of 370 km and is situated in the southeastern part of the Mediterranean (Figure 1). It lies geographically between the longitudes 29.2° and 32.6° E and latitudes 30.85° and 31.0° N. Nafaa *et al*. (1991) have characterized this region as a critical zone along the Northern coast, extending from Abu-Quir to Port-Said. This area frequently experiences severe winter storms, which substantially contribute to its annual sediment budget. Notably, in winter, the maximum recorded H_s reaches 4.0 m, predominantly from the WNW-NW direction, with fewer waves originating from the NNE-NE sector.

Moreover, El-Nahry and Doluschitz (2010), and Iskander (2013) reported that the wave climate in the Delta is influenced by several factors, including wind patterns, seasonal variations, and topography. Naffaa (1995) further emphasized the seasonality of wave conditions in the Delta. Specifically, from March to August, the region experiences relatively calm seas, whereas from September to February, the wave conditions become notably more intense.

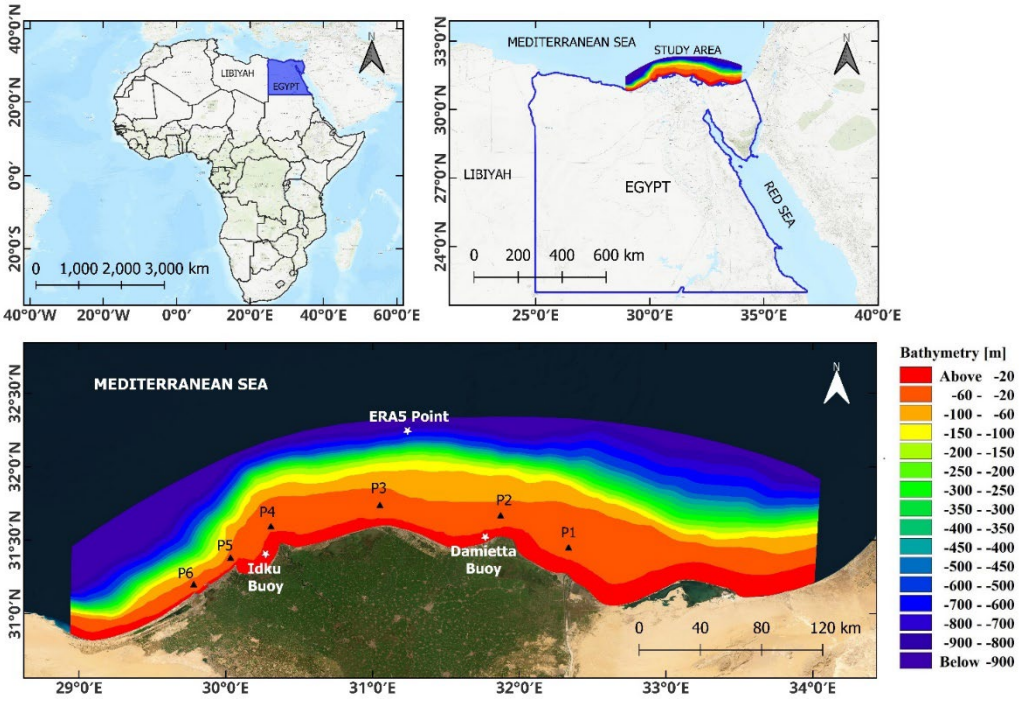

Figure 1. Study area, bathymetry map, model boundaries, buoy locations in the Nile Delta, and the selected locations

2.2. Data Assembly

During the data assembly phase, various datasets were gathered for the study area, including bathymetric maps, wind data, and wave data. Bathymetric maps were obtained from Admiralty charts, and contour lines in front of the Delta were extracted to represent the bathymetry of the study area.

Wind datasets were sourced from ERA5 for Rosetta and Damietta for the year 2017. Additionally, wind observations were obtained from Rosetta and Damietta for the same period. The observed wave data were extracted from the Idku Buoy for the period 2004-2005 and the Damietta Buoy for 2003-2004, as detailed in Table 1.

It is important to note that the ECMWF Reanalysis Project, conducted by the European Centre for Medium-Range Weather Forecasts "ECMWF", has produced several reanalysis datasets. ERA-15, the first analysis product, covered the period from 1978 to 1994. This was followed by ERA-40, which provided data from 1957 to 2002. Subsequently, ERA-Interim was released with data spanning 1979 to 2019. The most recent release, ERA5, offers high spatial resolution and covers the period from 1940 to 2023.

ERA5 benefits from reanalyzing historical data using a consistent system that incorporates archived data not available in earlier analyses. This advancement allows for the revision of historical maps, particularly in areas with sparse or uneven data coverage, and facilitates the creation of new maps incorporating atmospheric levels that were not previously considered.

Buoy	Instrument	Depth (m)	Period	Temporal resolutions	Number of Observations
Idku	S4DW	14.1	07.2004-12.2004	4-hour	1,110
			01.2005-11.2005		1,798
Damietta	S4DW	12	07.2003-12.2003	4-hour	1,777
			01.2004-07.2004		736

Table 1. Observed wave data from the Nile Delta

2.3. Numerical Modeling

The numerical modeling for this study was conducted using the MIKE 21-SW model. This section provides an overview of the historical and theoretical background of the MIKE 21-SW model, detailing its development and underlying principles. Additionally, the section outlines the calibration and validation processes employed to ensure the accuracy and reliability of the model. This involves a comprehensive explanation of the procedures used to adjust and test the model against the observed data. Furthermore, the section elaborates on the synthesis of the near-shore wave long-term data series. This synthesis integrates historical wave data to enhance the model's performance and provide a robust framework for analyzing wave conditions in the study area.

2.3.1. MIKE 21 Background

MIKE 21, developed by DHI, is a third-generation model designed for simulating 2-D wave dynamics. It utilizes a mesh that implements the cell-centered finite-volume technique based on differential equations governing wave behavior. Among its various modules, the Spectral Waves module stands out as a third-generation tool for spectral wind-wave simulations. This module is specifically designed to model the

transformation of waves driven by wind forces. The MIKE 21-SW module is versatile, capable of representing waves in different types of areas, including complex coastal and near-shore environments. The governing equations used in MIKE 21-SW are formulated for both the Cartesian and Polar coordinate systems, as described by Komen *et al.* (1994) and I. R. Young (1999). These equations provide the foundation for accurately simulating wave transformations and interactions. The following sections detail the specific governing equations used in MIKE 21-SW:

$$\frac{S}{\sigma} = \frac{\partial N}{\partial t} + \nabla(\vec{v}N) \qquad (1)$$

Where $N(\sigma, \theta, x, t)$ is action-density, t is time, x and y denote Cartesian-coordinates, $v = (c_\sigma, c_\theta, c_x, c_y)$ denotes propagation-velocity in 4-D, and ∇ is 4-D spatial differential operator (i.e., v, σ, and θ).

2.3.2. Set-up of MIKE 21-SW

To enhance the accuracy of the simulation, the region was discretized using a triangulated mesh that covers 48 km², with variable resolution tailored to both offshore and onshore conditions. This mesh consisting of 229,001 points and 454,965 triangles offers a highly detailed spatial representation essential for capturing the intricate coastal and bathymetric features. The use of variable resolution was crucial in balancing computational efficiency with the need for precision, ensuring that the complex dynamics of the region were accurately modeled.

In configuring the MIKE 21-SW model, special attention was given to the accurate simulation of wave conditions. Following the insights of Akpinar and León (2016), and Amarouche *et al.* (2019), the model meticulously incorporated critical factors such as bathymetry, wind persistence, and fetch, which are essential for precise wave modeling. Bathymetric data, sourced from Admiralty charts, served as the foundation for simulating wave interactions within the study area, as shown in Figure 1, which illustrates the bathymetry used for wave climate simulations and highlights the region's boundaries.

The model was driven by ERA5 reanalysis data, covering the period from 1940 to 2023, which provided realistic climate conditions updated every four hours. This comprehensive dataset included wind and wave parameters, ensuring a robust representation of historical climate variability. The JONSWAP formulation was employed to model the wave spectrum, essential for accurately capturing energy distribution in waves. The spectral formulation featured a directional frequency wave spectrum with 16 frequency bins, selected to encompass a wide range of wave directions and frequencies, ensuring a detailed representation of the wave climate. Model outputs included H_s and T_p at six specified locations.

2.4. Model Calibration and Validation

To evaluate the reliability of the ERA5 wind data from Rosetta and Damietta for the year 2017, a direct comparison was performed with the observed wind measurements from the same locations and periods. This comparison aimed to establish confidence in the ERA5 dataset. Subsequently, a comprehensive calibration and validation process was undertaken to ensure the accuracy of the MIKE 21-SW wave model results. Figure 2 illustrates the calibration and validation procedures for the MIKE 21-SW model. These steps were crucial for fine-tuning the model's parameters and ensuring its reliability for subsequent analysis.

Specifically, the calibration phase utilized wave data from buoys in Edku for the year 2004. In contrast, the validation phase employed wave data from buoys in Edku (2005) and Damietta (2003-2004). The selection of these datasets was based on their availability and relevance to the study area, providing a solid foundation for model assessment. During both phases, particular attention was given to the key parameters such as H_s and Tp, with the simulated values computed at the point nearest to the buoy locations. A critical aspect of the

calibration process involved the precise selection of the friction coefficient, a parameter that significantly influences wave propagation. Additionally, incorporating wave-breaking factors (γ and α) was essential to accurately simulate realistic wave behavior as these factors govern energy dissipation due to breaking waves.

To comprehensively assess the model's performance, two graphical tools were employed (i.e., Taylor diagrams and scatter plots). The Taylor diagrams provided a comparative overview by simultaneously displaying the normalized standard deviation and correlation coefficients between the simulated and observed data. This dual representation enabled a clear evaluation of the model's effectiveness in replicating real-world wave conditions. Additionally, scatter plots were used to illustrate the relationship between simulated and observed data points. The proximity of data clusters to the 45-degree line within these plots indicated the strength of the correlation, with a color scale further representing the density of these data points. These visual tools, when used in conjunction, provided a robust framework for evaluating the model's accuracy and consistency.

Moreover, the model's performance was quantitatively evaluated using several statistical metrics, including the correlation coefficient (CC), bias, Scatter Index (SI), Root-Mean-Square Error (RMSE), and Mean Absolute Error (MAE). The goal was to maximize the CC and minimize errors (RMSE, bias, and SI), thus offering comprehensive insights into the model's predictive accuracy. The equations used to compute these metrics are detailed in Equations 2 to 8. By meticulously calibrating and validating the MIKE 21-SW model, this study ensured that the simulated wave conditions closely matched the actual wave climate. This rigorous approach provides a reliable basis for further analysis and decision-making in coastal management.

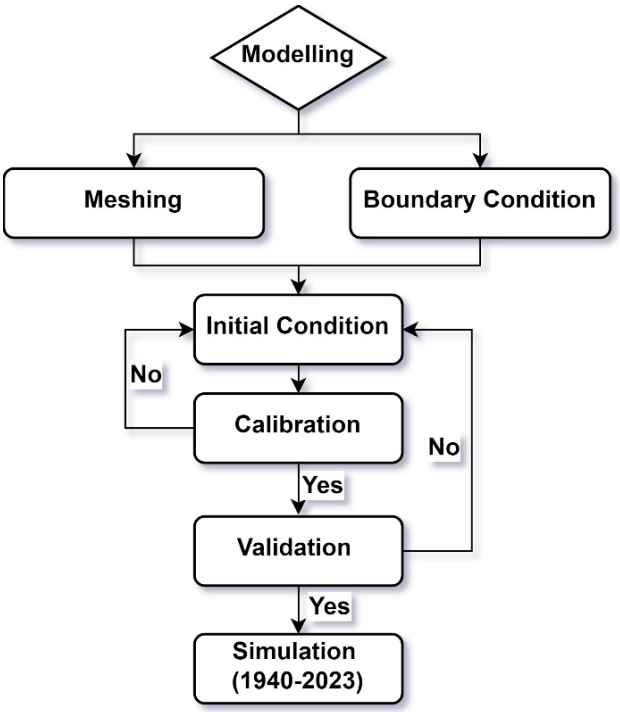

Figure 2. Flowchart for Calibration and Validation of MIKE21 SW Model

$$\bar{x} = \frac{1}{n}\sum_{i=1}^{n} x \qquad (2)$$

$$\bar{y} = \frac{1}{n}\sum_{i=1}^{n} y \qquad (3)$$

$$MAE = \frac{1}{n}\sum_{i=1}^{n} |y - x| \qquad (4)$$

$$RMSE = \sqrt{\frac{1}{n}\sum_{i=1}^{n}(y-x)^2} \quad (5)$$

$$BIAS = \frac{1}{n}\sum_{i=1}^{n}(y-\bar{x}) \quad (6)$$

$$SI = \frac{\sqrt{\frac{1}{n}\sum_{i=1}^{n}(y-x-BIAS)^2}}{\frac{1}{n}\sum_{i=1}^{n}|x_i|} \quad (7)$$

$$CC = \frac{\sum_{i=1}^{n}(x_i-\bar{x})(y_i-\bar{y})}{\sqrt{\sum_{i=1}^{n}(x_i-\bar{x})^2 \sum_{i=1}^{n}(y_i-\bar{y})^2}} \quad (8)$$

Where n represents the number of data, x is the measured value, y is the simulated value, and $\bar{x}$ and $\bar{y}$ represent the average values.

2.4.1. Evaluation of ERA5 Wind Data Accuracy

The observed wind data were contrasted against ERA5 data, and the results are depicted in Figure 3. This scatter plot illustrates the comparison of ERA5 versus observed wind data for Rosetta and Damietta. It reveals a strong alignment with the 45° line, indicating a high degree of correspondence between the two datasets.

To quantify this correspondence, several statistical metrics were employed. The analysis identified a slight bias of -0.38 m/s, indicating a minor underestimation in the ERA5 data. Additionally, the RMSE was calculated at 1.40 m/s, and the MAE was 1.09 m/s, both reflecting the average magnitude of discrepancies between observed and predicted values. Furthermore, the CC was found to be 0.90, demonstrating a strong positive correlation, while the SI was relatively low at 0.19%, highlighting the dataset's overall accuracy.

When these results are compared to previous studies in the region, such as those by Abu Zed *et al*. (2022), they reported a CC of 0.90, a Bias of -0.31 m/s, an RMSE of 1.25 m/s, and an SI of 0.26%, the ERA5 wind speed data used in this study show consistency. This alignment with earlier findings further validates the accuracy of the ERA5 data in capturing wind speeds for the area under investigation.

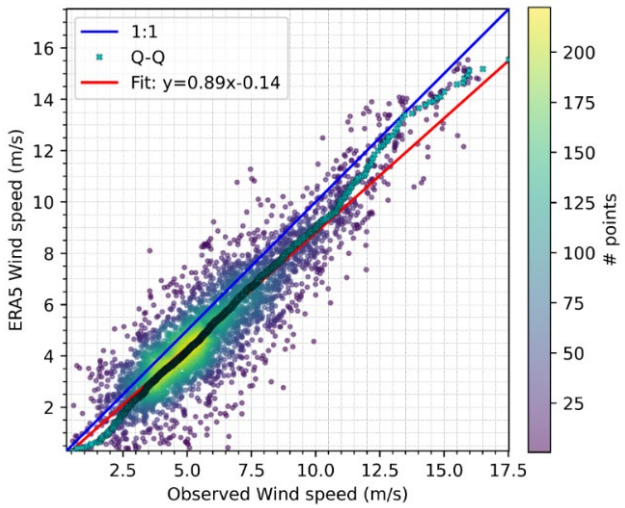

Figure 3. ERA5 wind speed versus observed wind speed at Rosetta and Damietta during 2017

2.4.2. Model Calibration

The calibration process was undertaken to fine-tune the parameters of the MIKE 21-SWmodel, specifically the spectral wave module. For this process, deep-water wave data from ERA5 were utilized, and near-shore wave data at Edku for the year 2004 were obtained using MIKE 21-SW. The results of the calibration process are presented in Figures 4 and 5. Among the various model runs, the 8th run was found to outperform the others. This conclusion is supported by the Taylor diagram in Figure 4, where the grouping of model runs shows the eighth run closest to the observation point. This proximity indicates a better agreement between the modeled and measured values compared to the other runs. The 8th run demonstrated a robust CC for both H_s and T_p, with values of 0.96 and 0.79, respectively. These high CC values indicate a strong fit between the simulated and observed data.

Moreover, the eighth run exhibited low RMSE values for H_s and T_p (0.15 m and 0.71 s, respectively), signifying minimal differences between predicted and actual values. The bias values for both parameters were close to zero (0.03 m for H_s and 0.01 s for T_p), indicating unbiased predictions. Additionally, the SI values showed negligible deviations from observed values (0.22% for H_s and 0.11% for T_p). Figure 5 presents scatter plots of observed and simulated H_s and T_p for the eighth run, showing a strong alignment along the 45-degree line for both parameters. This alignment further confirms the accuracy of the model in replicating the observed wave conditions. The 8th run's superior performance was achieved with the following calibration values: a friction coefficient of 0.001 m/s, α = 0.95, and γ = 0.8.

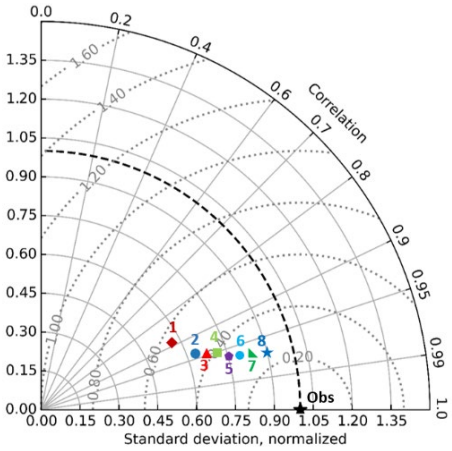

Figure 4. Taylor diagrams for observed and simulated H_s with varying bottom friction

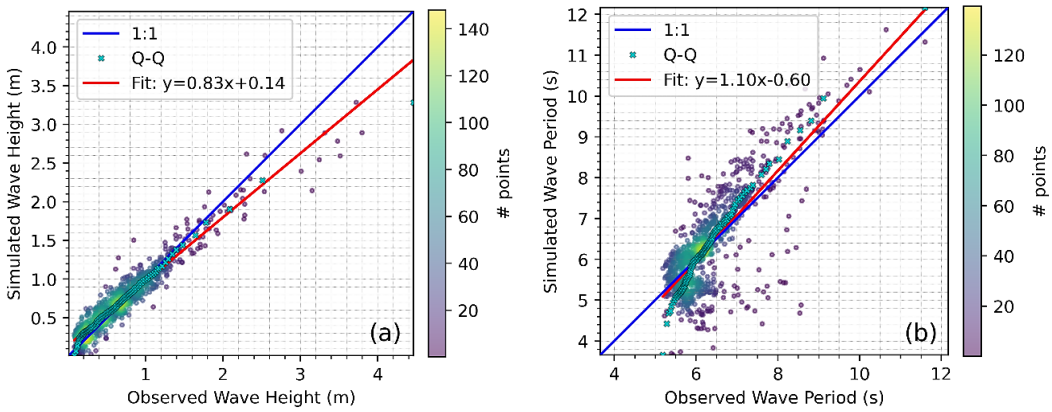

Figure 5. Results of the 8th calibration run: (a) H_s (m), and (b) T_p (s)

2.4.3. Model Validation

The validation process is essential for ensuring the credibility of the MIKE 21-SW model's results. To validate the model, deep-water wave data from ERA5 were utilized for Edku (2005) and Damietta (2003 and 2004). This step was crucial for instilling confidence in the model predictions. During this phase, the MIKE 21-SW module was applied, and near-shore wave data were obtained for the specified periods and locations. Subsequently, the model's output was compared against the measured data from the same locations and timeframes.

The validation results are summarized in Table 2, which lists the statistical parameters used to evaluate model accuracy. Additionally, Figure 6 illustrates the comparison between observed and simulated wave data for H_s and T_p. The close agreement between the observed and simulated data is evident from the high CC of 0.890 for H_s and 0.775 for T_p. These values indicate a strong correlation between the model predictions and actual observations.

Furthermore, the RMSE values were very low, at 0.055 for H_s and 0.168 for T_p, suggesting the minimal discrepancies between the model's outputs and the measured data. The SI values, 0.334 for H_s and 0.138 for T_p, also reflect the model's ability to accurately replicate the observed wave conditions. Collectively, these statistical measures indicate that the MIKE 21-SW model performed well during the validation process, accurately simulating the wave climate at the specified locations and time periods.

The comparison of these validation results with those from previous studies conducted in the Mediterranean region reveals consistency. For instance, Amarouche *et al*. (2019) reported Bias, RMSE, and SI values for simulated H_s as 0.04m, 0.31m, and 0.3%, respectively. Similarly, Abu Zed *et al.* (2022) used the SWAN model and ERA5 data to calculate Bias, RMSE, and SI metrics for simulated H_s as 0.06m, 0.22m, and 0.33%, and for T_p as 0.43s, 1.34s, and 0.18% respectively. Furthermore, Elkut *et al*. (2021) reported Bias, RMSE, and SI values for simulated H_s of -0.28m, 0.29m, and 0.31% respectively. These comparisons underscore the robustness of the MIKE 21-SW model performance and confirm its reliability in simulating wave climate in the regions studied.

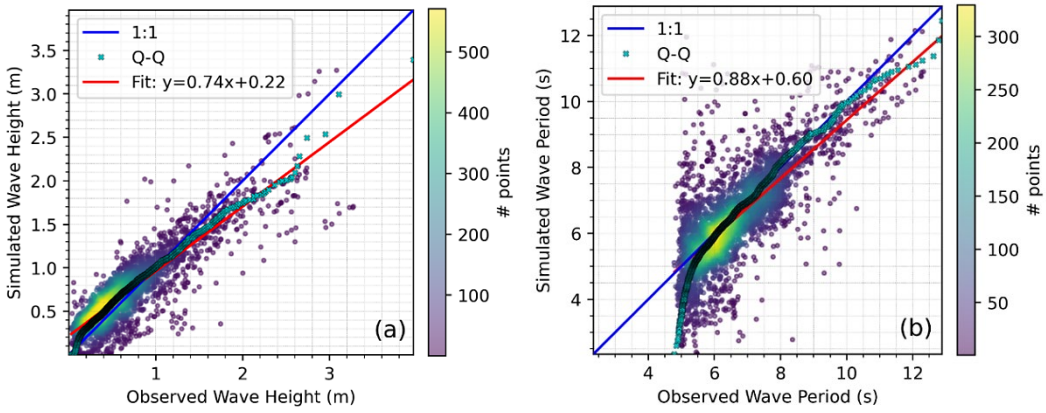

Figure 6. Results of the validation process: (a) H_s (m), (b) T_p (s)

Parameter	Bias	RMSE	MAE	SI (%)	CC
H_s (m)	0.055	0.219	0.162	0.334	0.890
T_p (s)	-0.168	0.923	0.644	0.138	0.775

Table 2. Model results versus buoy observations

2.5. Long-Term Analysis of Maximum Wave Height

Based on the MIKE 21-SW model's calibration and validation results, it was used to generate a long-term series of near-shore wave data spanning from 1940 to 2023 (i.e., 84 years). To conduct this analysis, six specific points were selected along the 20-meter depth contour line of the Nile Delta, where maximum wave limits were established at each location. This study utilizes three distinct time series analysis methods to identify long-term trends at the selected points along the Delta coast. These methods include linear regression, Theil-Sen estimation, and ElasticNet modeling. Each of these techniques provides unique insights into the long-term maximum H_s trends, which will be described in detail below.

2.5.1. Linear Regression

A linear regression was executed to the time series to obtain a seasonal trend and a monthly trend, where linear-regression equation, Equation (9), was utilized, in which 'a and b' were calculated using the least-square method.

$$y = a + b * t \tag{9}$$

where y is meteorological variable (i.e., H_s), t is time (year), a is regression coefficient (i.e., trend line intercept with y-axis), and b is slope coefficient.

2.5.2. Theil-Sen Estimation

The Theil-Sen estimation is a method for calculating the linear slope of two variables. Theil-Sen operates by gathering every potential pair of data points and calculating the slope of the line that connects them. Then, it uses the median of these slopes to estimate the true slope. This approach makes it resistant to outliers because the extreme values have less influence on the final estimate compared to the linear regression, which considers all the data points equally (Abdalla, Bidlot, and Breivik, 2015; Sen, 1968; Yue, Pilon, and Cavadias, 2002). The slope estimate formula is as follows:

$$Slop = \text{Median}\left(\frac{y_i - y_j}{t_i - t_j}\right) \tag{10}$$

Where y represents the H_s at the time tj and ti (tj>ti).

2.5.3. ElasticNet

ElasticNet combines the two most popular regularized linear regression types (i.e., ridge L2 and lasso L1). It prevents the need to choose between these two models by incorporating both the L2 and L1 approaches. ElasticNet is especially useful when working with multicollinear datasets, as it manages such scenarios by identifying a subset of relevant features while minimizing overfitting. The objective function is as follows:

$$Objective\ function = \frac{1}{2N}\sum_{i=1}^{N}(y_i - \hat{y}_i)^2 + \propto (\lambda_1 \|\beta\|_1 + \lambda_2 \|\beta\|_2^2) \tag{11}$$

Where N is the number of observations, yi is the actual response for observation, and $\hat{y}_i$ is the predicted response for observation. β is the vector of coefficients, and $\|\beta\|_1$ is its L1 norm (sum of absolute values). $\|\beta\|_2^2$ represents the coefficient vector's L2 norm (also known as the Euclidean norm or the square root of the sum of squares). The mixing parameter, α, defines the degree of regularization and typically ranges from 0 to 1. λ_1 and λ_2 represent the regularization parameters for L1 and L2 penalties respectively.

3. RESULTS ANALYSIS AND DISCUSSIONS

3.1. Wave Climate

The validation process of the MIKE 21-SW model, a well-regarded tool for simulating wave dynamics, was rigorously examined to ensure its accuracy. This examination revealed that the model effectively reproduced key wave parameters such as H_s and T_p, as confirmed by a thorough comparison with observational data. Such validation reinforces the model reliability in reflecting actual wave conditions.

By integrating ERA5 data with the MIKE 21-SW model, this study successfully created a comprehensive long-term wave data series, offering valuable insights into the wave climate of the region. Furthermore, Figure 7 vividly illustrates the directional distribution of simulated H_s at a depth of 20 meters. This figure not only highlights the predominant wave directions and their associated heights but also provides a detailed visualization of wave dynamics within the study area.

The predominant wave direction from the N-NW sector, observed 86% of the time, underscores the region's consistent wave climate, aligning with findings from previous studies (Abo Zed, 2007; Frihy, Abd El Moniem, and Hassan, 2002). Regarding the wave heights, the maximum recorded on the eastern side of the Delta is 4.94 meters, with an average H_s of 0.88 meters and an average T_p of 6.1 seconds. In contrast, the western side exhibits a maximum wave height of 6.35 meters, an average H_s of 0.96 meters, and a peak period of 6.13 seconds. Notably, wave heights typically remain below 1.22 meters for over 75% of the year. Additionally, wave periods between 2.0 and 6.1 seconds occur for more than half of the year, whereas longer periods exceeding 8.0 seconds are observed in less than 10% of the time.

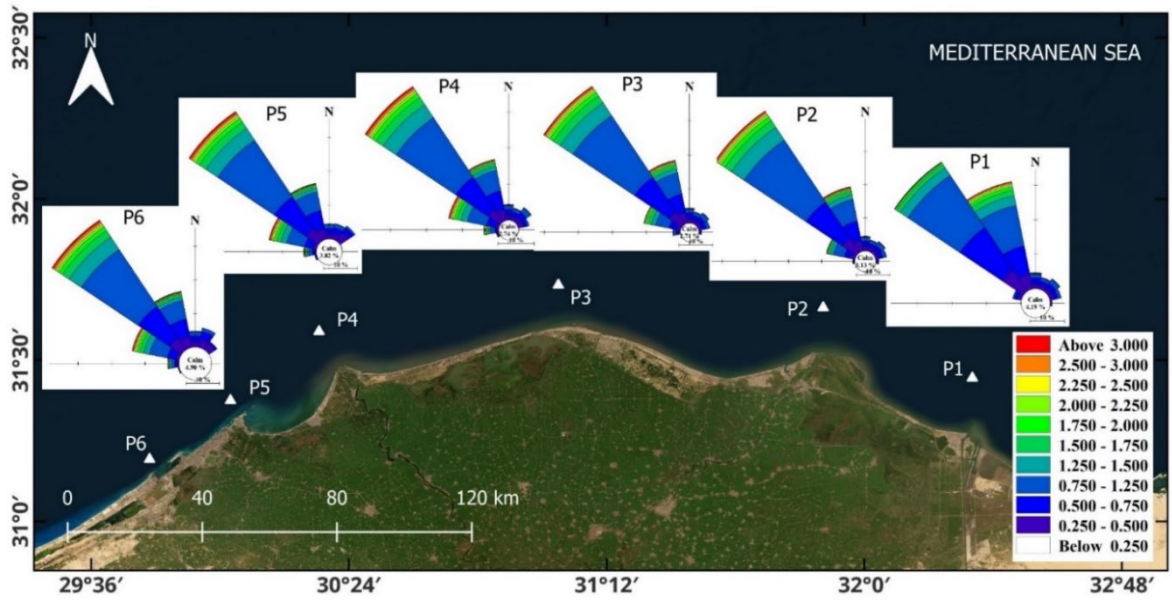

Figure 7. Simulated directional distribution of wave heights (m) in the Nile Delta from 1940 to 2023 at a depth of 20 m

3.2. Results Analysis and Discussion of Long-Term Data

The results of the analysis of the synthesized long-term series of near-shore wave data during 84 years (i.e., 1940-2023), where the three methods were used to obtain the seasonal-trend and monthly-trend. Long-

term wave changes are characterized by maximum H_s trends from 1940–2023. This is presented and explained in detail below.

3.2.1. Seasonal Analysis

This section investigates seasonal trends in the maximum H_s along the Nile Delta coast. The results of the synthesized long-term wave data were analyzed, where the seasonal trend was obtained by linear-regression, Thil-Sen and ElasticNet methods. For example, Figure 8 shows the H_s trends during the winter at selected locations along the Nile Delta coastline. It shows that the winter season has a positive trend in all locations using the three methods. However, the trend values varied between the locations; for example, linear-regression method reported trend values ranging from 0.15 cm/year at P1 to 0.53 cm/year at P6. In contrast, Thil-Sen method reported trend values ranging from 0.21 cm/year at P1 to 0.67 cm/year at P6. Furthermore, the ElasticNet method provided trend values ranging from 0.07 cm/year at P1 to 0.45 cm/year at P6.

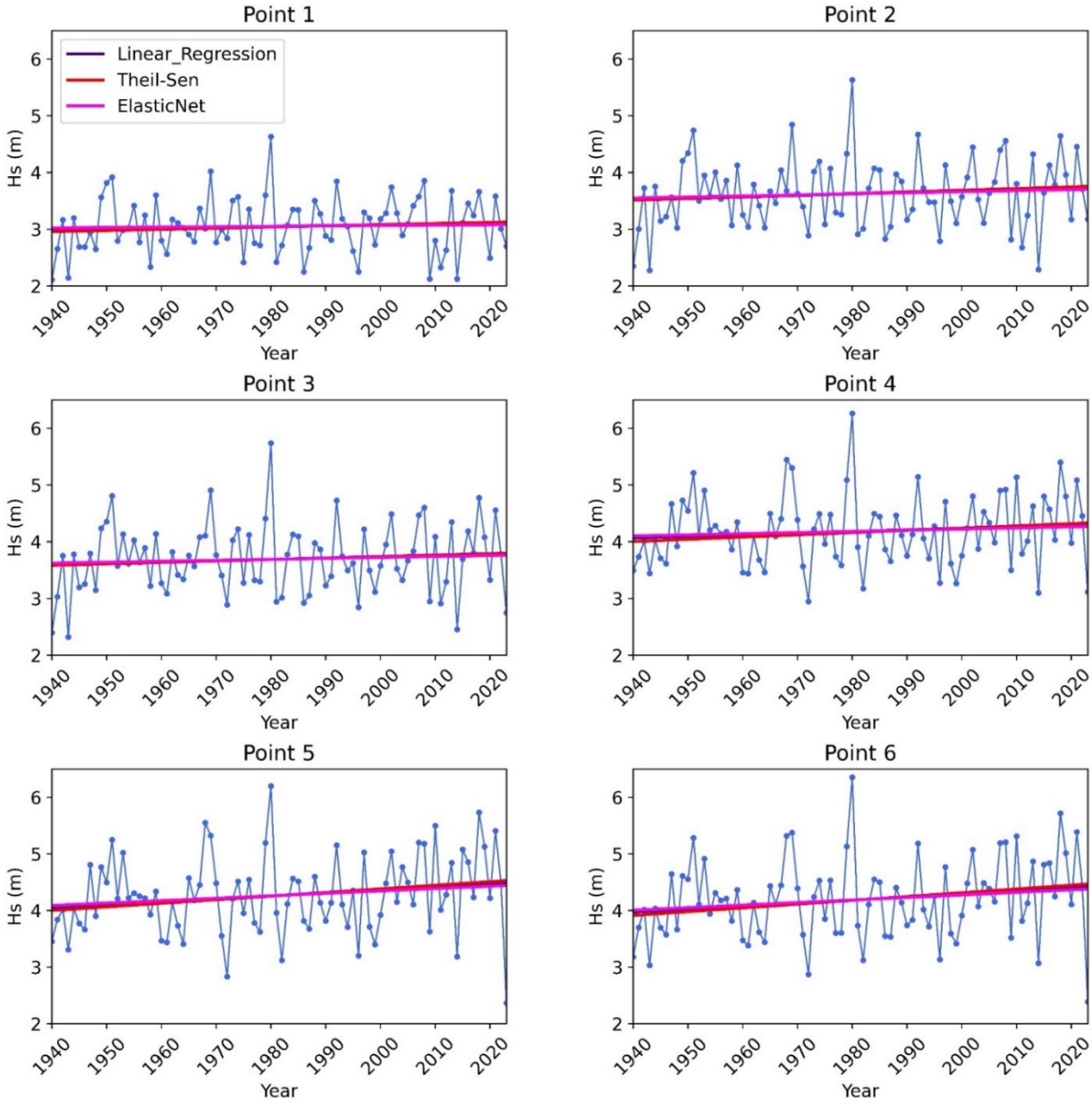

Figure 8. Seasonal trends for the maximum H_s time series in winter by using the three methods at each of the six selected points

Figure 9 presents the seasonal Hs trend for each of the six investigated points, where it was apparent that the seasonal trend of Hs varies seasonally. It is worth noting that neither spring nor winter show any negative trend, which implies a consistent pattern of rising Hs during these seasons. In contrast, there is a negative trend in the maximum Hs at most sites in the summer. For instance, during the summer, sites P1–P4 showed negative trend values, while P5 and P6 showed small positive trends. Notably, Thil-Sen method consistently produced higher trend values across all locations than either the linear-regression or ElasticNet, especially in winter and spring. For example, in spring, Linear Regression had trend values ranging from 0.17 to 0.30 cm/year, Theil-Sen from 0.21 to 0.40 cm/year, and ElasticNet from 0.09 to 0.22 cm/year. Furthermore, the ElasticNet method noticed no trends in specific locations during the summer and autumn seasons. Specifically, during the summer, there was no trend at locations 2, 3, 5, and 6. Similarly, during the autumn season, locations 2, 3, and 4 showed no distinct trend.

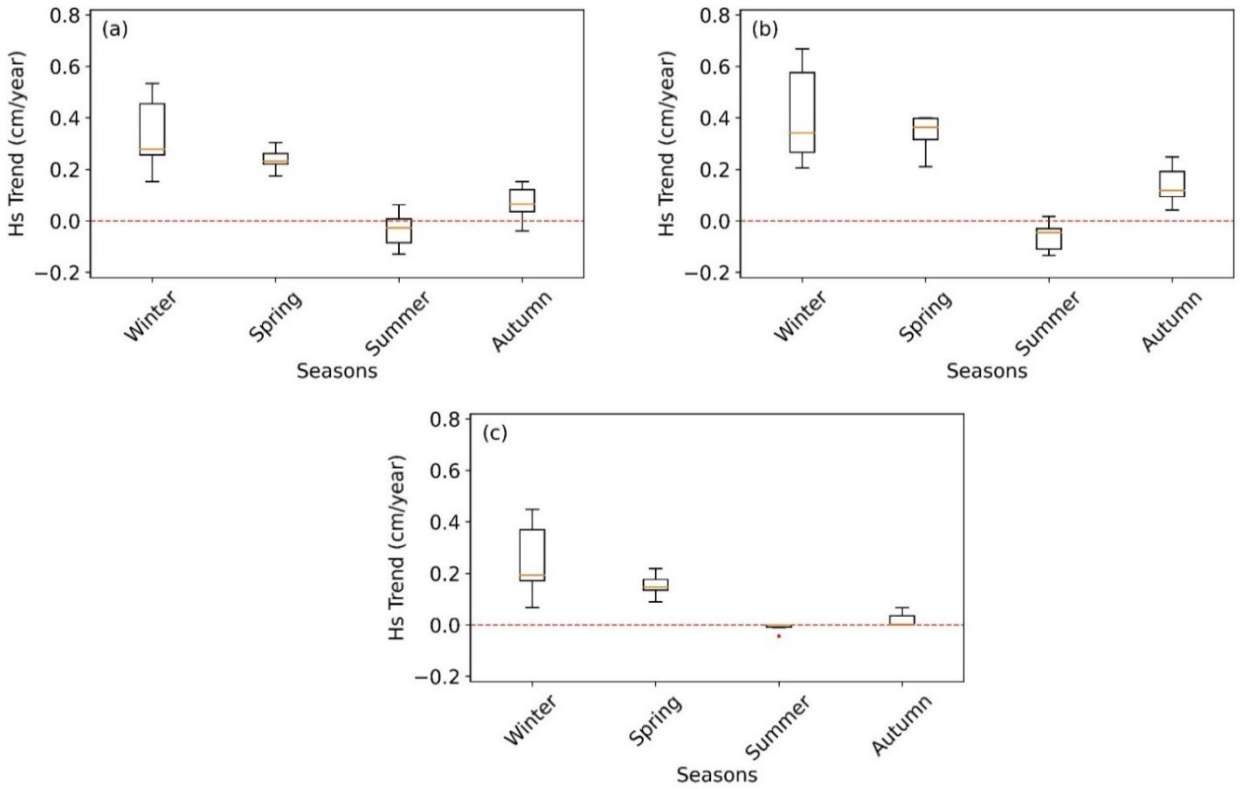

Figure 9. Box plot of seasonal variation trends with the maximum H_s: (a) Linear-regression, (b) Thil-Sen, and (c) ElasticNet

3.2.2. Monthly Analysis

The results of the produced long-term wave data set (by MIKE21-SW) were analyzed (to obtain a monthly-trend) and presented in Figures 10 and 11. Figure 10 shows the trends in the maximum H_s during January at selected locations along the Nile Delta coastline. The figure shows a positive trend in January across all locations using the three methods. However, there were differences in the trend values between these locations. For example, the linear-regression method reported trend values ranging from 0.17 cm/year at P4 to 0.43 cm/year at P2. In contrast, Thil-Sen method reported trend values ranging from 0.08 cm/year at P4 to 0.40 cm/year at P2. Furthermore, the ElasticNet method provided trend values ranging from 0.08 cm/year at P4 to 0.34 cm/year at P2.

Figure 11 presents the monthly H_s trend representing the 6 investigated points, where it is apparent that the monthly-trend of H_s varies monthly. For example, in February, the trend values ranged from 0.20 to 0.55 cm/year for linear regression, 0.23 to 0.52 cm/year for Theil-Sen method, and 0.20 to 0.52 cm/year for ElasticNet. March shows additional differences, with trend values ranging from 0.02 to 0.41 cm/year for Theil-Sen method, 0.05 to 0.34 cm/year for linear-regression, and 0 to 0.28 cm/year for ElasticNet. It is worth noting that all months, with the exception of July, August, and September, show a positive trend. In August, all the three methods showed a negative trend in most locations, with slight variations in trend values. Linear regression showed trend values between -0.19 and 0.03 cm/year, while Theil-Sen method suggested a range of -0.23 to -0.04 cm/year. ElasticNet, on the other hand, displayed trend values ranging from -0.23 to -0.01 cm/year.

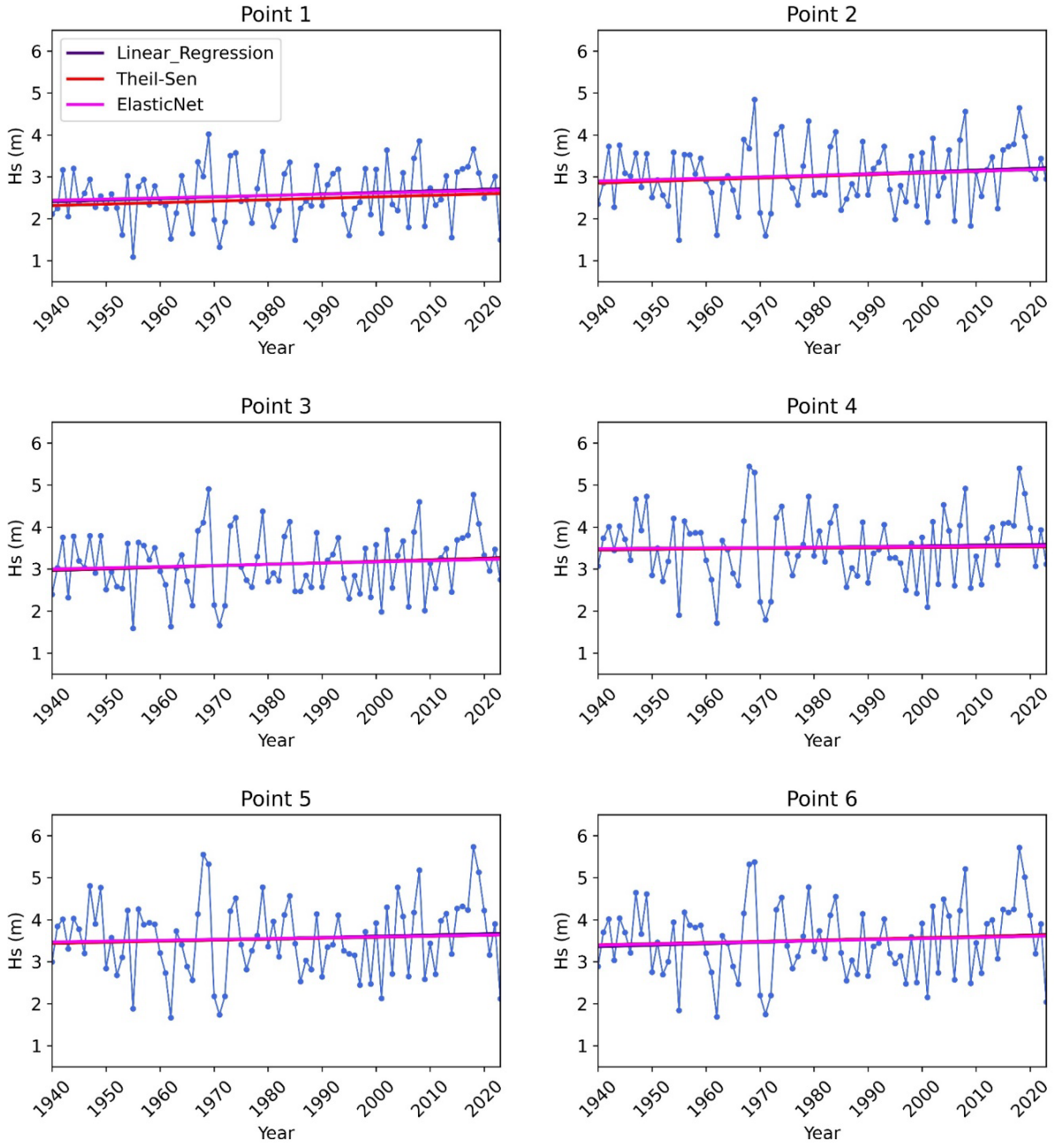

Figure 10. Monthly trends for maximum H_s time series in January estimated using three different methods at each of the six selected points

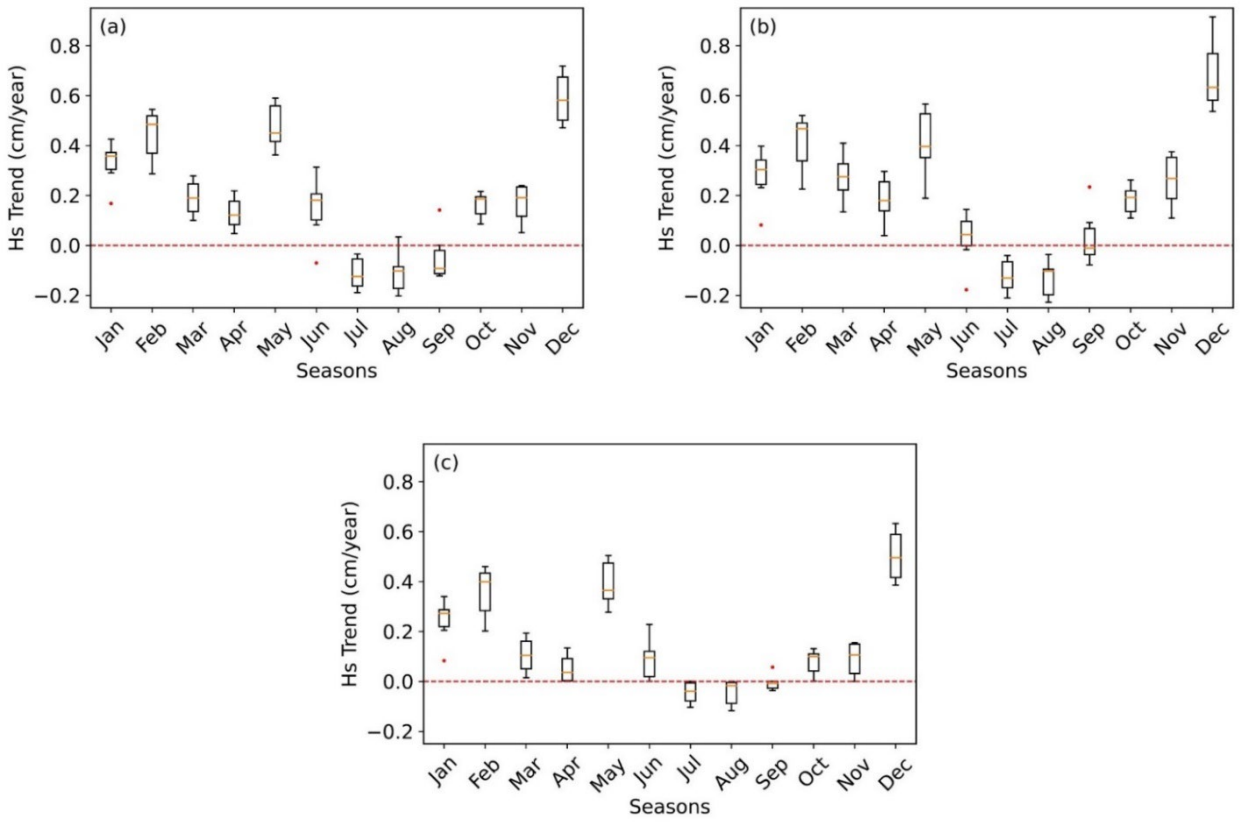

Figure 11. Estimated Monthly trend variation of maximum H_s: (a) Linear Regression, (b) Thil-Sen, (c) ElasticNet

The analysis of the long-term wave data along the Nile Delta coastline offers valuable insights into the trends and variations in the maximum H_s over an extended period (1940-2023). The synthesized data allowed the examination of seasonal and monthly trends using three analytical methods: linear-regression, Thil-Sen, and ElasticNet. Notably, no negative trends were observed during the spring or winter seasons, suggesting that H_s increased during these periods. Conversely, most sites exhibited a negative trend in the maximum H_s during the summer, with only a few locations showing slight positive trends.

Furthermore, the examination of monthly trends provides additional insights into the temporal variability along the Nile Delta coastline. Distinct patterns emerged, with the majority of months showing positive trends in the maximum H_s, except for July, August, and September. It is important to note that the trend values varied across methods and locations; specifically, Thil-Sen consistently reported higher trend values compared to linear-regression and ElasticNet. This discrepancy could reflect seasonal variations in the wave dynamics, potentially influenced by factors such as weather patterns and coastal morphology.

Comparing these results with the global studies on H_s trends reveals notable consistencies. For instance, research by Young *et al.* (2011) identified a positive trend in maximum H_s across most of the world's oceans. Similarly, Ruggiero *et al*. (2010) observed a positive trend in the Pacific Ocean, with an increase in the mean annual H_s. Maia, Almeida, Nicolodi *et al*. (2023) reported significant increases in the wave heights in the Atlantic Ocean over the recent decades. In the Indian Ocean, Zheng and Li (2017) documented a notable increase in the monthly H_s during the 45-year period from 1957 to 2008. In the Mediterranean region, comparisons are also instructive. Barbariol *et al.* (2021) found that trend values for the maximum H_s were negative in summer and positive in winter over a 40-year study period (1980-2019). Similarly, Aristodemo *et al.* (2024) reported increased maximum H_s values over 42 years (1979-2020) in a significant portion of the Mediterranean Sea.

4. CONCLUSIONS AND RECOMMENDATIONS

This study investigates the vulnerability of coastal zones due to climate change, with a particular emphasis on the maximum H_s along the Nile Delta coast. An 84-year dataset from ERA5 was thoroughly analyzed to comprehensively examine historical wave patterns, utilizing the MIKE21 SW model, which was rigorously validated against the observed data. Based on the analyzed results, the following conclusions were deduced:

- The findings underscore a significant influence of climate change on the wave dynamics along the Nile Delta coast, with a pronounced trend of increasing maximum Hs, particularly during the winter months.
- The observed rise in the wave heights increases the risks of coastal erosion, flooding, and infrastructure damage, highlighting the urgent need for adaptive coastal management strategies to protect and sustainably develop these vulnerable areas.
- The statistical analyses reveal consistent long-term increasing trends in the maximum H_s across various methods, corroborating broader climate projections and affirming the strong impact of climate change on the wave dynamics.
- The ongoing increases in the wave heights may alter the return periods of the extreme sea states, which has implications for coastal planning and infrastructure resilience.
- It is imperative to incorporate future ocean wave climate trends into the design of marine structures to mitigate the increased risks associated with climate change, ensuring the longevity and safety of coastal infrastructure.
- Proactive coastal management is crucial in addressing the challenges posed by climate change and safeguarding coastal zones against future climate threats.

CONFLICT OF INTEREST

The authors declared no potential conflicts of interest with respect to the research, authorship, and/or publication of this article.

REFERENCES

Abdalla, S., Bidlot, J.R. & Breivik, Ø. 2015, 'Marine Wind and Wave Height Trends at Different ERA-Interim Forecast Ranges', Journal of Climate, 28(2), pp. 819–837. Available at: https://doi.org/10.1175/JCLI-D-14-00470.1.

Abo Zed, A.B. 2007, 'Effects of Waves and Currents on the Siltation Problem of Damietta Harbour, Nile Delta Coast, Egypt', Mediterranean Marine Science, 8(2), pp. 33–48. Available at: https://doi.org/10.12681/mms.152.

Abu Zed, A.A., Kansoh, R.M., Iskander, M.M. & Elkholy, M. 2022, 'Wind and Wave Climate Southeastern of the Mediterranean Sea Based on a High-Resolution SWAN Model', Dynamics of Atmospheres and Oceans, 99, pp. 101311. Available at: https://doi.org/10.1016/j.dynatmoce.2022.101311.

Akpinar, A. & León, S.P. 2016, 'An Assessment of the Wind Re-Analyses in the Modelling of an Extreme Sea State in the Black Sea', Dynamics of Atmospheres and Oceans, 73, pp. 61–75. Available at: https://doi.org/10.1016/j.dynatmoce.2015.12.002.

Albanai, J.A. 2020, 'Sea level rise projections for Failaka island in the state of Kuwait', Transactions on Maritime Science, 9(2), pp. 236–247. Available at: https://doi.org/10.7225/toms.v09.n02.008.

Amarouche, K., Akpınar, A., Bachari, N.E.I., Çakmak, R.E. & Houma, F. 2019, 'Evaluation of a high-resolution wave hindcast model SWAN for the West Mediterranean basin', Applied Ocean Research, 84(January), pp. 225–241. Available at: https://doi.org/10.1016/j.apor.2019.01.014.

Amarouche, K., Akpınar, A. & Semedo, A. 2022, 'Wave Storm Events in the Western Mediterranean Sea over Four Decades', Ocean Modelling, 170, 101933. Available at: https://doi.org/10.1016/j.ocemod.2021.101933.

Aristodemo, F., Loarca, A.L., Besio, G. & Caloiero, T. 2024, 'Detection and Quantification of Wave Trends in the Mediterranean Basin', Dynamics of Atmospheres and Oceans, 105, 101413. Available at: https://doi.org/10.1016/j.dynatmoce.2023.101413.

Aucan, J. 2018, 'Effects of Climate Change on Sea Levels and Inundation Relevant to the Pacific Islands What is Already Happening?', Pacific Marine Climate Change Report Card, pp. 43–49.

Aydoğan, B. & Ayat, B. 2018, 'Spatial Variability of Long-Term Trends of Significant Wave Heights in the Black Sea', Applied Ocean Research, 79(October 2017), pp. 20–35. Available at: https://doi.org/10.1016/j.apor.2018.07.001.

Barbariol, F., Davison, S., Falcieri, F.M., Ferretti, R., Ricchi, A., Sclavo, M. & Benetazzo, A. 2021, 'Wind Waves in the Mediterranean Sea: An ERA5 Reanalysis Wind-Based Climatology', Frontiers in Marine Science, 8(November), pp. 1–23. Available at: https://doi.org/10.3389/fmars.2021.760614.

Caloiero, T., Aristodemo, F. & Ferraro, D.A. 2022, 'Annual and Seasonal Trend Detection of Significant Wave Height, Energy Period and Wave Power in the Mediterranean Sea', Ocean Engineering, 243(October 2021), 110322. Available at: https://doi.org/10.1016/j.oceaneng.2021.110322.

Cannaby, H. & Hüsrevolu, Y.S. 2009, 'The influence of low-frequency variability and long-term trends in north Atlantic sea surface temperature on Irish waters', ICES Journal of Marine Science, 66(7), pp. 1480–1489. Available at: https://doi.org/10.1093/icesjms/fsp062.

Chowdhury, P., Behera, M.R. & Reeve, D.E. 2019, 'Wave Climate Projections along the Indian Coast', International Journal of Climatology, 39(11), pp. 4531–4542. Available at: https://doi.org/10.1002/joc.6096.

De Leo, F., Briganti, R. & Besio, G. 2024, 'Trends in Ocean Waves Climate Within the Mediterranean Sea: A Review', Climate Dynamics, 62(2), pp. 1555–1566. Available at: https://doi.org/10.1007/s00382-023-06984-4.

El-Nahry, A.H. & Doluschitz, R. 2010, 'Climate Change and its Impacts on the Coastal Zone of the Nile Delta, Egypt', Environmental Earth Sciences, 59(7), pp. 1497–1506. Available at: https://doi.org/10.1007/s12665-009-0135-0.

Elkut, A.E., Taha, M.T., Abu Zed, A.B.E., Eid, F.M. & Abdallah, A.M. 2021, 'Wind-Wave Hindcast using Modified ECMWF ERA-Interim Wind Field in the Mediterranean Sea', Estuarine, Coastal and Shelf Science, 252(February), 107267. Available at: https://doi.org/10.1016/j.ecss.2021.107267.

Elshinnawy, A.I. & Antolínez, J.A.Á. 2023, 'A Changing Wave Climate in the Mediterranean Sea during 58-Years using UERRA-MESCAN-SURFEX High-Resolution Wind Fields', Ocean Engineering, 271, 113689.

Frihy, O.E., Abd El Moniem, A.B. & Hassan, M.S. 2002, 'Sedimentation Processes at the Navigation Channel of the Damietta Harbour on the Northeastern Nile Delta Coast of Egypt', Journal of Coastal Research, 18, pp. 459–469.

Grabemann, I. & Weisse, R. 2008, 'Climate Change Impact on Extreme Wave Conditions in the North Sea: An Ensemble Study', Ocean Dynamics, 58(3), pp. 199–212. Available at: https://doi.org/10.1007/s10236-008-0141-x.

Hemer, M.A., Fan, Y., Mori, N., Semedo, A. & Wang, X.L. 2013, 'Projected Changes in Wave Climate from a Multi-Model Ensemble', Nature Climate Change, 3(5), pp. 471–476. Available at: https://doi.org/10.1038/nclimate1791.

Ibrahim, A.S.A., El Molla, A.M. & Ahmed, H.G.I. 2024, 'Modeling Longshore Sediment Transport for Sustainable Coastal Management in the Damietta Port Area', Journal of ETA Maritime Science, 12(2), pp. 116–127. Available at: https://doi.org/10.4274/jems.2024.35119.

IPCC 2013, Climate Change 2013: The Physical Science Basis. Contribution of Working Group I to the Fifth Assessment Report of the Intergovernmental Panel on Climate Change, Stocker, T.F., Qin, D., Plattner, G.-K., Tignor, M., Allen, S.K., Boschung, J., Nauels, A., Xia, Y., Bex, V. & Midgley, P.M. (eds.), Cambridge University Press, Cambridge, UK.

Iskander, M.M. 2013, 'Wave Climate and Coastal Structures in the Nile Delta Coast of Egypt', Emirates Journal for Engineering Research, 18(1), pp. 43–57.

Knobler, S., Liberzon, D. & Fedele, F. 2022, 'Large Waves and Navigation Hazards of the Eastern Mediterranean Sea', Scientific Reports, 12(1), pp. 1–17. Available at: https://doi.org/10.1038/s41598-022-20355-9.

Komen, G.J.L., Cavaleri, M., Donelan, K., Hasselmann, S. & PAEM, J. 1994, Dynamics and Modelling of Ocean Waves, Cambridge University Press, Cambridge, UK.

Kovačić, M. & Favro, S. 2024, 'Analysis of Beaches and Beach Managing in Context of New Maritime Domain and Sea Ports Act', Transactions on Maritime Science, 13(1). Available at: https://doi.org/10.7225/toms.v13.n01.017.

Lionello, P., Bhend, J., Buzzi, A., Krichak, S.O., Jansa, A., Maheras, P. & Lisboa, U. De. 2006, 'Cyclones in the Mediterranean Region: Climatology and Effects on the Environment', in Mediterranean Climate Variability, pp. 325–372.

Maia, N.Z., Almeida, L.P., Nicolodi, J.L., Calliari, L. & Castelle, B. 2023, 'Long-Term Trends and Wave Climate Variability in the South Atlantic Ocean: The Influence of Climate Indices', Regional Studies in Marine Science, 66, 103131. Available at: https://doi.org/10.1016/j.rsma.2023.103131.

Mentaschi, L., Vousdoukas, M.I., Voukouvalas, E., Dosio, A. & Feyen, L. 2017, 'Global Changes of Extreme Coastal Wave Energy Fluxes Triggered by Intensified Teleconnection Patterns', Geophysical Research Letters, 44(5), pp. 2416–2426. Available at: https://doi.org/10.1002/2016GL072488.

Nafaa, M., Fanos, A. & Elganainy, M. 1991, 'Characteristics of Waves off the Mediterranean Coast of Egypt', Journal of Coastal Research, 7(3), pp. 665–676.

Naffaa, M. 1995, 'Wave Climate Along the Nile Delta Coast', Journal of Coastal Research, 11(1), pp. 219–229. Available at: https://doi.org/10.1080/03056249708704247.

Pang, T., Wang, X., Nawaz, R.A. et al. 2023, 'Coastal Erosion and Climate Change: A Review on Coastal-Change Process and Modeling', Ambio, 52, pp. 2034–2052. Available at: https://doi.org/10.1007/s13280-023-01901-9.

Ruggiero, P., Komar, P.D. & Allan, J.C. 2010, 'Increasing Wave Heights and Extreme Value Projections: The Wave Climate of the U.S. Pacific Northwest', Coastal Engineering, 57(5), pp. 539–552. Available at: https://doi.org/10.1016/j.coastaleng.2009.12.005.

Saraçoğlu, K., Ari Güner, H., Şahin, C., Yüksel, Y. & Çevik, E. 2016, 'Evaluation of the Wave Climate over the Black Sea: Field Observations and Modeling', Coastal Engineering, pp. 2013–2015. Available at: https://doi.org/10.9753/icce.v35.waves.20.

Satterthwaite, D. 2007, The Transition to a Predominantly Urban World and Its Underpinnings, Human Settlements Discussion Paper Series: Urban Change-4.

Sen, P.K. 1968, 'Estimates of the Regression Coefficient Based on Kendall's Tau', Journal of the American Statistical Association, 63(324), pp. 1379–1389. Available at: https://doi.org/10.1080/01621459.1968.10480934.

Shi, J., Feng, X., Toumi, R., Zhang, C., Hodges, K.I., Tao, A. & Zheng, J. 2024, 'Global Increase in Tropical Cyclone Ocean Surface Waves', Nature Communications, 15(1), 174. Available at: https://doi.org/10.1038/s41467-023-43532-4.

Simav, Ö., Şeker, D.Z. & Gazioğlu, C. 2013, 'Coastal Inundation Due to Sea Level Rise and Extreme Sea State and Its Potential Impacts: Çukurova Delta Case', Turkish Journal of Earth Sciences, 22(4), pp. 671–680. Available at: https://doi.org/10.3906/yer-1205-3.

Soukissian, T., Karathanasi, F., Axaopoulos, P., Voukouvalas, E. & Kotroni, V. 2018, 'Offshore Wind Climate Analysis and Variability in the Mediterranean Sea', International Journal of Climatology, 38(1), pp. 384–402. Available at: https://doi.org/10.1002/joc.5182.

Wang, X.L. & Swail, V.R. 2002, 'Trends of Atlantic Wave Extremes as Simulated in a 40-yr Wave Hindcast Using Kinematically Reanalyzed Wind Fields', Journal of Climate, 15(9), pp. 1020–1035.

Young, I.R. 1999, Wind Generated Ocean Waves, Elsevier. Available at: https://api.semanticscholar.org/CorpusID:129891655.

Young, I.R., Babanin, A.V. & Zieger, S. 2011, 'Response to Comment on "Global Trends in Wind Speed and Wave Height"', Science, 334(6058), pp. 10–12. Available at: https://doi.org/10.1126/science.1210548.

Young, I.R. & Ribal, A. 2019, 'Multiplatform Evaluation of Global Trends in Wind Speed and Wave Height', Science, 364(6440), pp. 548–552. Available at: https://doi.org/10.1126/science.aav9527.

Yue, S., Pilon, P.J. & Cavadias, G. 2002, 'Power of the Mann–Kendall and Spearman's RHO Tests for Detecting Monotonic Trends in Hydrological Series', Journal of Hydrology, 259, pp. 254–271. Available at: https://doi.org/10.1016/S0022-1694(01)00594-7.

Zheng, C.W. & Li, C.Y. 2017, 'Analysis of Temporal and Spatial Characteristics of Waves in the Indian Ocean Based on ERA-40 Wave Reanalysis', Applied Ocean Research, 63, pp. 217–228. Available at: https://doi.org/10.1016/j.apor.2017.01.014.